ACS OMEGA

Article

Cite This: ACS Omega 2017, 2, 6975-6983

http://pubs.acs.org/journal/acsodf

Immunosensor for Pancreatic Cancer Based on Electrospun Nanofibers Coated with Carbon Nanotubes or Gold Nanoparticles

Juliana C. Soares,[†] Leonardo E. O. Iwaki,[†,‡] Andrey C. Soares,[†,‡] Valquiria C. Rodrigues,[†] Matias E. Melendez,[§] José Humberto T. G. Fregnani,[§] Rui M. Reis,[§,∥] Andre L. Carvalho,[§] Daniel S. Corrêa,[⊥] and Osvaldo N. Oliveira, Jr.*[,†]

[†]São Carlos Institute of Physics, University of São Paulo, 13560-60 São Carlos, Brazil

[‡]Department of Materials Engineering, São Carlos School of Engineering, University of São Paulo, 13563-120 São Carlos, Brazil

[§]Molecular Oncology Research Center, Barretos Cancer Hospital, 14784-400 Barretos, Brazil

[∥]ICVS/3B's-PT Government Associate Laboratory, Life and Health Sciences Research Institute (ICVS), University of Minho, 4710-057 Braga, Portugal

[⊥]Nanotechnology National Laboratory for Agriculture (LNNA), Embrapa Instrumentação, 13560-970 São Carlos, Brazil

ABSTRACT: We report the fabrication of immunosensors based on nanostructured mats of electrospun nanofibers of polyamide 6 and poly(allylamine hydrochloride) coated either with multiwalled carbon nanotubes (MWCNTs) or gold nanoparticles (AuNPs), whose three-dimensional structure was suitable for the immobilization of anti-CA19-9 antibodies to detect the pancreatic cancer biomarker CA19-9. Using impedance spectroscopy, the sensing platform was able to detect CA19-9 with a detection limit of 1.84 and 1.57 U mL^{-1} for the nanostructured architectures containing MWCNTs and AuNPs, respectively. The high sensitivity achieved can be attributed to the irreversible adsorption between antibodies and antigens, as confirmed with polarization-modulated infrared reflection absorption spectroscopy. The adsorption mechanism was typical Langmuir−Freundlich processes. The high sensitivity and selectivity of the immunosensors were also explored in tests with blood serum from patients with distinct concentrations of CA19-9, for which the impedance spectra data were processed with a multidimensional projection technique. The robustness of the immunosensors in dealing with patient samples without suffering interference from analytes present in biological fluids is promising for a simple, effective diagnosis of pancreatic cancer at early stages.

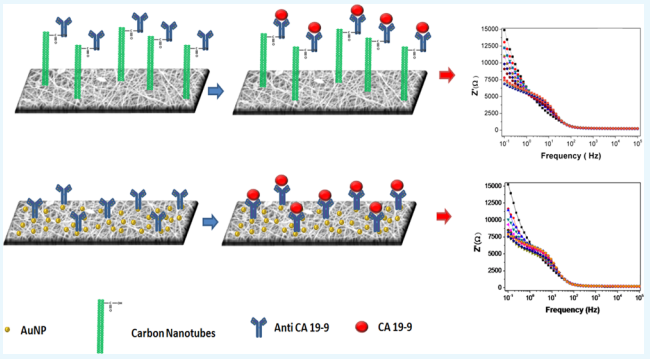

1. INTRODUCTION

Immunosensors based on the molecular recognition process between antibodies and antigens have been developed since the 1960s[1−3] upon exploiting physicochemical processes similar to the enzyme-linked immunosorbent assay.[4] These sensors have been used for a variety of diseases with a number of detection principles, including electrochemical techniques,[5] optical,[6] and magneto-optical methods.[7] Common to all of these immunosensors is the need to immobilize either antibodies or antigens on the sensing units, which must preserve their activity for sufficiently long periods of time and allow for the binding of the corresponding molecule in the antibody−antigen pair. This requirement is normally fulfilled by controlling the molecular architecture of the nanostructured films of which most immunosensors are made.[8−10] In addition to the active layer containing antibodies or antigens, the nanostructured films contain a matrix designed to assist in preserving bioactivity and other components (e.g., nanomaterials) to enhance sensitivity.[11] Experimental methods such as the self-assembled monolayer,[12,13] layer-by-layer,[14] and Langmuir−Blodgett[15−17] techniques have been employed owing to their suitability to build complex molecular architectures, where synergy may be sought among the properties of the nanomaterials comprising the immunosensors.

The extensive list of nanomaterials that can be utilized in immunosensors includes graphene,[18−21] carbon nanotubes (CNTs),[22−26] carbon nanoballs, metallic nanoparticles,[26] and nanostructures derived from natural resources, for example, chitosan,[27] and electrospun polymer nanofibers.[28,29] Such nanomaterials are normally used with a twofold purpose. On one hand, they serve as a matrix for immobilizing the biomolecules, but they can also be exploited to enhance the sensitivity by increasing the measured signal. This is the case of carbon nanotubes whose chemical, thermal, mechanical, and electrical properties make them suitable for biosensing,[30] especially with functionalization by carboxylic acid groups

Received: July 19, 2017
Accepted: October 5, 2017
Published: October 19, 2017

DOI: 10.1021/acsomega.7b01029
ACS Omega 2017, 2, 6975−6983

that allow for interaction with molecules containing amino groups. Gold nanoparticles (AuNPs) are also used to amplify the analytical signal either because a higher electric current can be generated or because they provide a larger number of active sites in a single recognition reaction.[31] These nanomaterials can be further combined with polymer-based nanostructured architecture such as those made with electrospun polymer films.[23] The advantages of using electrospun nanofibers, in particular, are associated with cost-effective method to produce a tridimensional platform of large specific surface area, high porosity, and one-dimensional confinement characteristics.[32] These features can be beneficial for immobilizing biomolecules with preserved activity and enhancing sensitivity.

In this article, we explore the use of electrospun nanofibers combined with carbon nanotubes (CNTs) and gold nanoparticles (AuNPs) to produce immunosensors for detecting the biomarker CA19-9, referred to as Lewis antigen, which is the only biomarker approved by the Food and Drug Administration of the United States for pancreatic cancer.[33−35] The choice of this biomarker was based on two factors: (i) on one hand, biosensors to detect pancreatic cancer at early stages seem today the only possible avenue to reduce the mortality rate of this type of cancer, which at present reaches 99.3% of the patients.[36] This high rate is caused by the difficulty of early diagnosis because the disease is silent in most patients and by the lack of effective treatments;[10] (ii) on the other hand, we shall be able to compare the immunosensors performance with similar ones reported in the literature, as there has been considerable efforts to develop sensors for detecting CA19-9,[10,34,37−39] including from our group.[10] With regard to the use of AuNPs and CNTs, the aim was to test the suitability of the combination with the electrospun nanofibers because these nanomaterials can promote enhanced electron transfer and increase biosensor sensitivity.[23,40,41] We have not used neat polyamide 6 (PA6)/poly(allylamine) (PAH) nanofibers because they are not amenable to be functionalized for an efficient adsorption of the antibodies.

Detection of CA19-9 is made here with electrochemical impedance spectroscopy in the samples where the antigen is added to a buffer at different concentrations and in samples of blood serum from the patients of a cancer hospital. To achieve selectivity in such complex samples as those of blood serum, the impedance spectra data are treated with a multidimensional projection technique.[42] Furthermore, because we aim at establishing generic platforms for immunosensors that can be extended to other types of cancer, we investigate the formation of nanofiber mats and sensing mechanisms using the surface-specific techniques scanning electron microscopy (SEM) and polarization-modulated infrared reflection absorption spectroscopy (PM-IRRAS).

2. RESULTS AND DISCUSSION

2.1. Detection of CA19-9 Biomarker. The immunosensors with the two architectures based on PA6/PAH nanofibers, modified with MWCNT or AuNPs, were both capable of detecting the antigen CA19-9 in the buffer solutions, as demonstrated in the electrochemical impedance spectra in Figure 1a,c. The difference in the real component of the impedance is particularly relevant at low frequencies, consistent with the results of similar immunosensors, as the electrical signal below 100 Hz is normally dominated by the double-layer effects.[43] The CA19-9 concentration dependence is best represented by plotting the change in the real component of

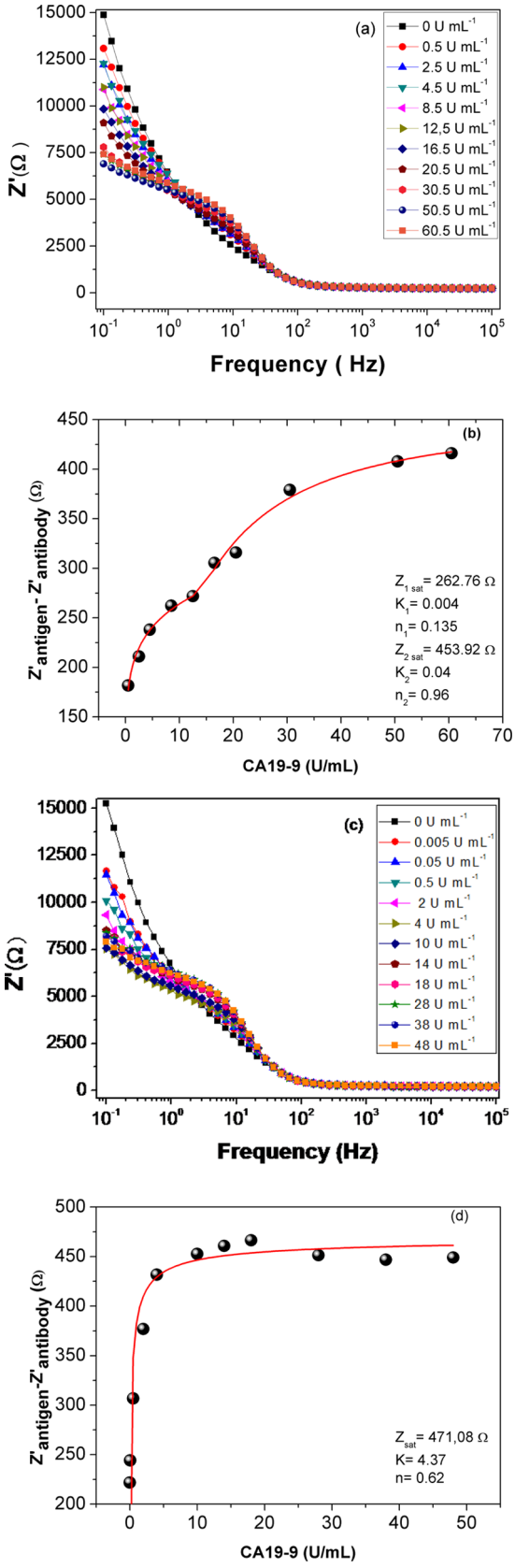

Figure 1. Electrochemical impedance spectra for indium tin oxide (ITO) electrodes modified with PA6/PAH/MWCNT/anti-CA19-9 (a) and PA6/PAH/AuNPs/anti-CA19-9 (c) in $K_3Fe(CN)_6$ and in $K_4Fe(CN)_6$. Change in the real component of the impedance vs CA19-9 concentration for PA6/PAH/MWCNT/anti-CA19-9 (b) and PA6/PAH/AuNPs/anti-CA19-9 (d) architectures. The solid curves

DOI: 10.1021/acsomega.7b01029
ACS Omega 2017, 2, 6975−6983

Figure 1. continued

were calculated with one Langmuir−Freundlich isotherm in (d) and a combination of two Langmuir−Freundlich isotherms in (b). The parameters used for the fitting are the adsorption capacity of the system (taken as proportional to the change in impedance), Z_{sat}, the affinity constant for adsorption K, and the heterogeneity index n.

the impedance Z' at 10 Hz, which increases sharply at low concentrations before saturation when all of the available anti-CA19-9 antibody sites are occupied by the adsorption of CA19-9 molecules. The adsorption mechanisms can be explained by using the Langmuir−Freundlich isotherms, as discussed in the next subsection.

The major difference between the two nanostructured architectures lies in the lower limit of detection and the lower concentration for saturation of the PA6/PAH/AuNPs/anti-CA19-9 (Figure 1d) architecture. Indeed, for the PA6/PAH/MWCNT/anti-CA19-9 architecture, the calibration curve in Figure 1b may be approximated by a straight line up to ca. 4.5 U mL^{-1}, whereas the corresponding linear region for PA6/PAH/AuNPs/anti-CA19-9 is up to 2 U mL^{-1}. As for the sensitivity, determined using the International Union of Pure and Applied Chemistry method,[44] the limit of detection was 1.84 and 1.57 U mL^{-1} for PA6/PAH/MWCNT/anti-CA19-9 and PA6/PAH/AuNPs/anti-CA19-9, respectively. These limits of detection are lower than those quoted for the commercial sensors Architect i2000 (2 U mL^{-1})[45] and AxSYM (2 U mL^{-1})[45] and competitive with the commercial sensors KRYPTOR (1.2 U mL^{-1})[45] and Elecsys (0.6 U mL^{-1})[45] and immunosensors made with Au/porous graphene nanocomposites matrix (0.006 U mL^{-1}),[46] Au−SiO_2/Fe_3O_4 nanospheres (0.01 U mL^{-1}),[47] and the sensor made with chitosan/concanavaline A matrix (0.69 U mL^{-1}).[10]

In addition to being capable of distinguishing different concentrations of the biomarker, immunosensors need to be selective for a particular biomarker. This means that the immunosensors should be robust against possible interferents commonly present in biological fluids, such as in blood serum samples. The results in Figure 2 demonstrate the robustness of the two immunosensors, which are not affected when exposed to glucose, ascorbic acid, and fetal bovine serum, with tests performed following the same procedures as in the detection results. In the presence of the interferents, Z' is close to the value for the control sample of phosphate-buffered saline (PBS). In contrast, there was a clear increase for the two samples containing 2 and 48 U mL^{-1} in Figure 2a and 2.5 and 40 U mL^{-1} in Figure 2b of CA19-9 biomarker. The difference is particularly significant for the PA6/PAH/AuNPs/anti-CA19-9 immunosensors, which confirms their higher sensitivity inferred from the detection limit calculated with data in Figure 1d.

It is significant that the two immunosensors could perform successfully with real samples extracted from the blood serum of four patients from Barretos Cancer Hospital. To offer a visual demonstration, we treated the impedance spectra acquired with these patient samples with a multidimensional projection technique referred to as Interactive Document Map (IDMAP).[42] In this type of data treatment, each measured spectrum is represented by a circle on the two-dimensional IDMAP plot, with the positioning being defined according to the similarity of the spectra, given by eq 1.

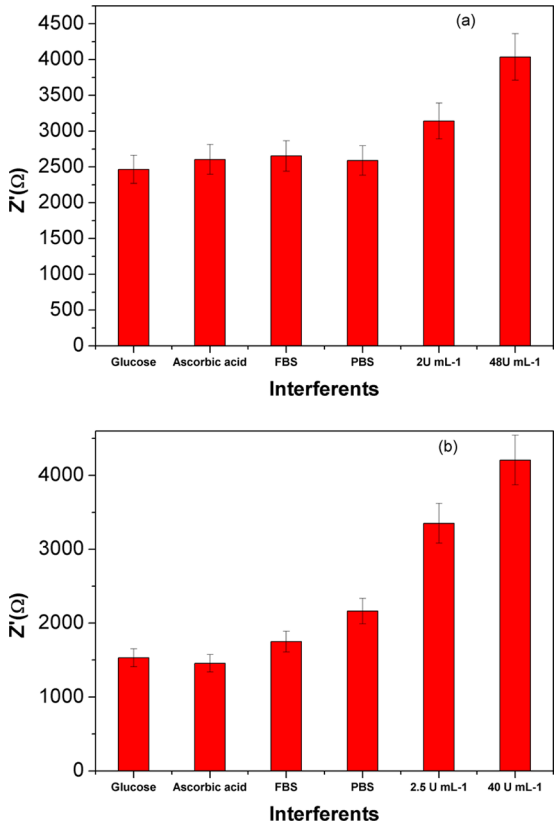

Figure 2. Difference in the real component of the impedance for an immunosensor made with (a) PA6/PAH/MWCNT/anti-CA19-9 and (b) PA6/PAH/AuNPs/anti-CA19-9 architectures exposed to PBS and various analytes introduced in PBS.

$$S_{\mathrm{IDMAP}} = \frac{\delta(x_i, x_j) - \delta_{\min}}{\delta_{\max} - \delta_{\min}} - d(y_i, y_j) \quad (1)$$

where $\delta_{\max}$ and $\delta_{\min}$ are the maximum and minimum distances between data instances, $\delta(x_i, x_j)$ is the distance between two samples in the original space, and $d(y_i, y_j)$ is the distance function on the projected space. That is to say, similar spectra are placed close to each other on the projected space. Figure 3 shows that patients whose blood serum has a high CA19-9 concentration (likely to develop pancreatic cancer) can be easily distinguished from the patients with lower CA19-9 concentrations.

2.2. Adsorption Mechanisms Behind Biosensing. It is now well established that the high sensitivity and selectivity of immunosensors are ascribed to the irreversible adsorption of the detected antigens (or antibodies) on immobilized antibodies (or antigens).[9,10] This has been proven for cancer biomarkers as well, as exemplified with different types of experimental methods, including nanogravimetry,[48] PM-IRRAS,[9,10] and scanning electron microscopy (SEM).[48] In this study, we also probed these adsorption mechanisms and established models that account for the impedance experimental data.

SEM images of the nanofibers coated with MWCNTs and AuNPs are shown in Figure 4a,d, respectively. Two images of the same nanofibers mats were taken and shown to display the same qualitative surface characteristics. Of note are typical[23] 200 nm diameter electrospun nanofibers decorated with MWCNTs in Figure 4a and a uniform coating of 18 nm

DOI: 10.1021/acsomega.7b01029
ACS Omega 2017, 2, 6975−6983

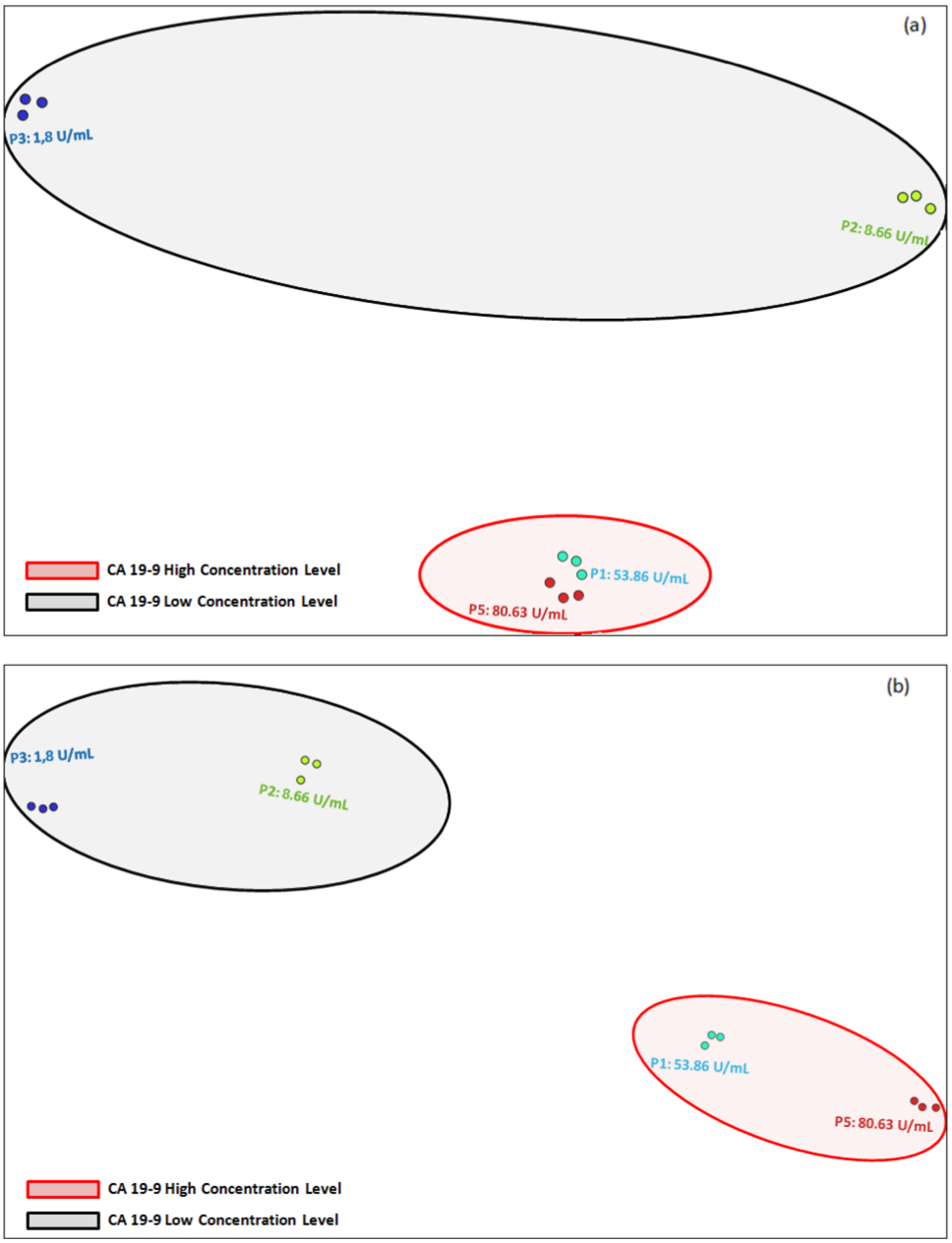

Figure 3. IDMAP plots obtained from the impedance spectra of four serum samples from the patients in Barretos Cancer Hospital using the sensing units: (a) PA6/PAH/MWCNTs/anti-CA19-9 and (b) PA6/PAH/AuNPs/anti-CA19-9. The axes are not labeled because in IDMAP plots what matters is the relative distance between data points. That is to say, the closer the points are on the plot, the more similar the corresponding impedance spectra are.

AuNPs in Figure 4d, consistent with the literature.[44] When these nanofibers were coated with a layer of anti-CA19-9 antibodies, the morphology changed entirely with irregularly shaped objects occupying most of the image (see Figure 4b,e). This applies to both nanofibers architectures, indicating that the adsorption of the antibody layer predominates as far as morphology is concerned. The SEM images of the PA6/PAH/MWCNTs/anti-CA19-9 and PA6/PAH/AuNPs/anti-CA19-9 architectures obtained after the nanofibers mats were exposed to a given CA19-9 concentration are shown in Figure 4c,f, respectively. The concentration chosen was 40 U mL^{-1}, close to the saturation of the anti-CA19-9 sites, according to the results in Figure 1b,d. The PA6/PAH nanofibers now appear coated with layers of biomarker, giving rise to fibers with no defined shape in both cases. The adsorption of anti-CA19-9 (Figure 4e) produces spherical clusters, which bind to gold nanoparticles. After the addition of 40 U mL^{-1} of CA19-9 biomarker (Figure 4f), as in the previous images, the PA6/PAH fibers lost their defined shape. This image was obtained with 30 000 times magnification to allow for the visualization of the fiber coating.

Interpretation of the SEM images provides evidence of the adsorption of CA19-9 antigen biomarkers, but it does not suffice to determine which chemical groups were involved in such adsorption. This can be reached by analyzing the PM-IRRAS spectra in Figure 5, where the baseline correction was made by taking the nanofibers mats of PA6/PAH/MWCNTs and PA6/PAH/AuNPs as reference. The adsorption of the

DOI: 10.1021/acsomega.7b01029
ACS Omega 2017, 2, 6975−6983

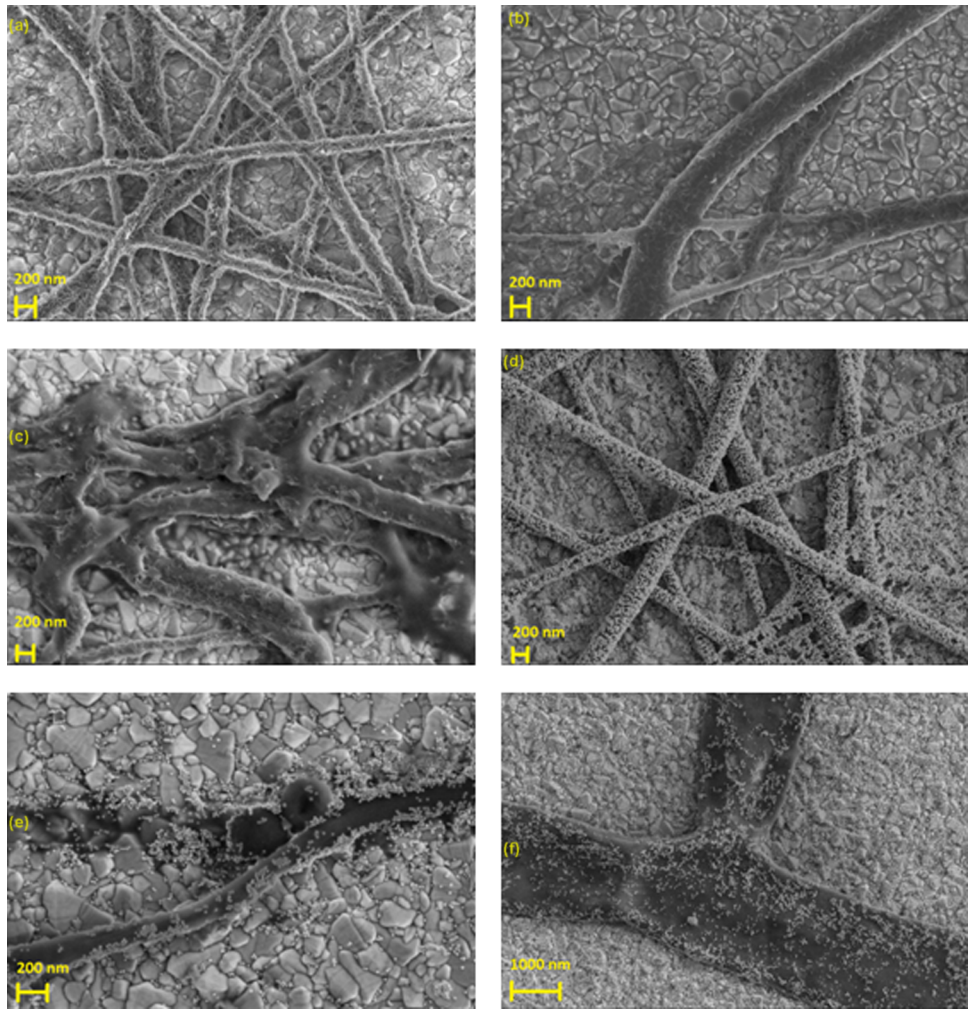

Figure 4. SEM images of nanofibers mats of (a) PA6/PAH/MWCNTs; (b) PA6/PAH/MWCNTs/anti-CA19-9; (c) PA6/PAH/MWCNTs/anti-CA19-9/40 U mL^{-1} biomarker; (d) PA6/PAH/AuNPs; (e) PA6/PA6/AuNPs/anti-CA19-9; and (f) PA6/PAH/AuNPs/anti-CA19-9/40 U mL^{-1} biomarker.

bioactive layer of anti-CA19-9 antibodies could perhaps be expected to lead to identical spectra. However, a comparison of the spectra for 0 U mL^{-1} in Figure 5a,b points to the differences because the number of anti-CA19-9 molecules adsorbed and their organization depend on the functionalized substrate. In the spectra, the most prominent bands are (i) amide I between 1600 and 1700 cm^{-1} assigned to vibrational modes of carbonyl (C═O) from the carboxylic acid groups in the amino acids; (ii) amide II between 1500 and 1600 cm^{-1}, where 60% of the vibration is associated with the N−H bond, whereas the remaining 40% is related to the C−N bond stretching of the amide groups. The bands are all directed upward, which means that the dipole moments of the groups involved are preferably oriented on the film plane. Because the bands in this region of the spectrum originate from proteins, all of them were affected by exposing the anti-CA19-9 lying on the active layer to the CA19-9 biomarker. The intensity of PM-IRRAS bands depends on the orientation as well as the number of functional groups giving rise to a specific band. Therefore, in some cases, adsorption of increasing amounts of analyte leads to a linear increase in band intensity, as occurred with amide I bands from CA19-9 in previous works to allow for a quantitative analysis.[8,49] With the PA6/PAH/MWCNTs/anti-CA19-9 and PA6/PAH/AuNPs/anti-CA19-9 immunosensors, however, there was no monotonic dependence on the concentration, and a quantitative analysis cannot be performed. Also relevant is the confirmation that CA19-9 was indeed adsorbed on the two film architectures, as indicated in the spectra of Figure 5c.

A quantitative analysis of the adsorption mechanisms is normally made by plotting the so-called adsorption isotherms, that is, the amount of adsorbed material versus the concentration of the adsorbate. For biosensors, there is evidence that the change in impedance (or capacitance) can be taken to be proportional to the mass of adsorbate.[9,10,48] In spite of the size of the antigens and complexity of antigen−antibody interactions, adsorption isotherms for immunosensors have been modeled with the simple Langmuir−Freundlich model,[9,10] originally developed for the adsorption of gas molecules on a surface. For the two nanofiber architectures investigated here, we attempted to fit the calibration curves in Figure 1b,d with Langmuir and Langmuir−Freundlich models available in the literature.[50−54] Equation 2 representing the Langmuir−Freundlich model yielded a good fitting in Figure 1d for CA19-9 adsorption on PA6/PAH/AuNPs/anti-CA19-9 architecture.

$$q = \frac{Q_{sat}(K \times C_{eq})^n}{(K \times C_{eq})^n + 1} \quad (2)$$

DOI: 10.1021/acsomega.7b01029
ACS Omega 2017, 2, 6975−6983

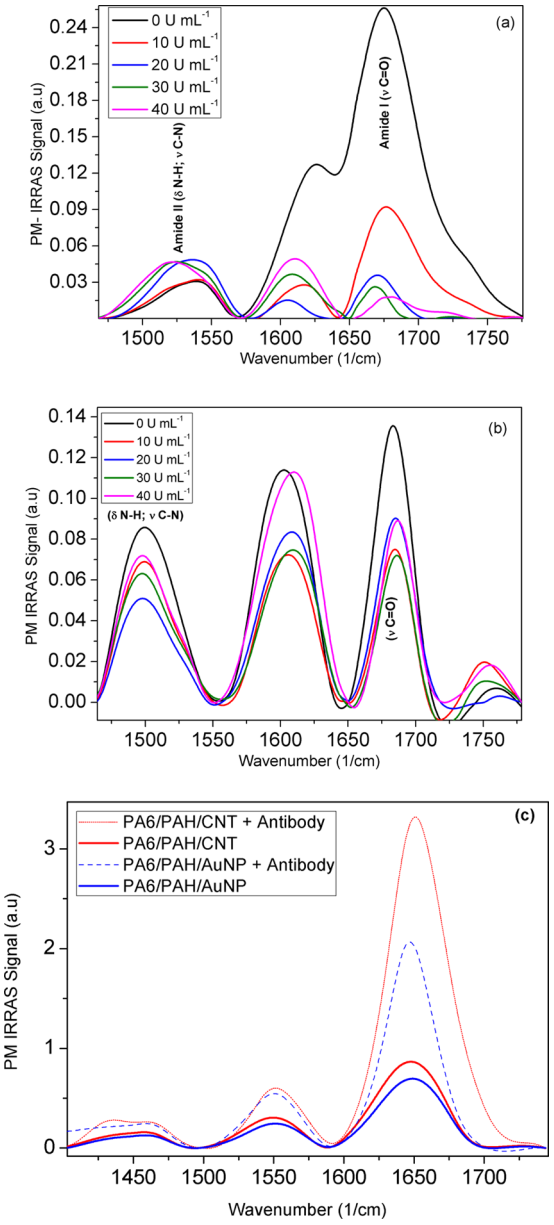

Figure 5. (a) PM-IRRAS spectra for the PA6/PAH/MWCNTs/anti-CA19-9 and (b) PA6/PAH/AuNPs/anti-CA19-9 architectures adsorbed on gold, before (black line) and after exposure to CA19-9 at various concentrations (colored lines). Baseline correction was performed by taking the spectra of the PA6/PAH/MWCNTs and PA6/PAH/AuNPs architectures as the background. (c) Adsorption of the antibodies on the PA6/PAH/MWCNTs and PA6/PAH/AuNPs films is proven by comparing the spectra with and without CA19-9 antibody, where the baseline correction was made using the gold substrate as background.

where q is taken as the amount of adsorbed material on the substrate at an equilibrium, proportional to the change in impedance, Q_{sat} is the adsorption capacity, K is the affinity constant for adsorption, C_{eq} is the aqueous phase concentration at equilibrium, and n is the index of heterogeneity. In contrast, for PA6/PAH/MWCNT/anti-CA19-9 architecture, adsorption of the CA19-9 biomarker in Figure 1b could only be achieved with a combination of two Langmuir–Freundlich functions (eq 3)

$$q = \frac{Q1_{sat}(K1 \times C1_{eq})^{n_1}}{(K1 \times C1_{eq})^{n_1} + 1} + \frac{Q2_{sat}(K2 \times C2_{eq})^{n_2}}{(K2 \times C2_{eq})^{n_2} + 1} \quad (3)$$

where the symbols have the same meaning as in eq 2, now with the subindices 1 and 2 denoting the two Langmuir–Freundlich processes. With the data we have available, it is not possible to determine why two adsorption processes are present before saturation. This result for the architecture containing MWCNTs differs from all of the the others reported in the literature, for which only one Langmuir–Freundlich process is observed.

3. CONCLUSIONS

Electrospun polymer nanofibers of PA6/PAH modified with either MWCNTs or AuNPs were used as matrix for the immobilization of anti-CA19-9 antibodies, which served as immunosensors to detect CA19-9 biomarker using electrochemical impedance spectroscopy. The nanostructured architectures showed high sensitivity in detecting the commercial CA19-9 in a buffer and for distinguishing blood serum samples of patients with distinct concentrations of the biomarker. The three-dimensional structure of the electrospun nanofibers, as revealed with SEM images, appears to be relevant for the successful preservation of the antibody activity. This high sensitivity and selectivity toward CA19-9 in the presence of interferents may be attributed to the antibody–antigen irreversible adsorption, which was confirmed here with PM-IRRAS spectroscopy in which amide bands were affected by exposure of the immunosensors to CA19-9. The adsorption process, in particular, is typical of Langmuir–Freundlich processes. The clear distinction of blood serum samples of the patients likely to develop pancreatic cancer from those with smaller CA19-9 concentrations, below the value considered as threshold (37 U mL^{-1}), was achieved by treating the electrochemical impedance data with a multidimensional projection technique. This is a limitation of the present study because a calibration curve for a quantitative analysis cannot be obtained in a straightforward manner. Future experiments with a larger number of blood serum samples are therefore required for generating sufficient data to which regression analysis methods can be applied to yield a quantitative determination of CA19-9 concentrations. An avenue will then be open for a simple, fast diagnosis of pancreatic cancer at early stages using an immunosensor platform that can also be utilized for other diseases.

4. EXPERIMENTAL SECTION

4.1. Preparation of PA6 and PA6/PAH Nanofibers.

Polyamide 6 (PA6), poly(allylamine) (PAH), and multiwalled carbon nanotubes (MWCNTs) were purchased from Sigma-Aldrich. The antibody anti-CA19-9 and the antigen CA19-9 were purchased from Aviva System Biology, whereas real samples of pancreatic cancer patients were provided by Barretos Cancer Hospital. Sera from the pancreatic cancer patients were quantified using the electrochemiluminescence analyzer model Cobas 601 (Roche Diagnostics, Indianapolis) and an Elecsys CA19-9 Immunoassay kit (Roche Diagnostics, Indianapolis). The use of patient serum samples was approved by the Committees on Ethics in Research of Barretos Cancer Hospital (Ethics Committee number 1.447.041).

PA6/PAH nanofibers were produced by the electrospinning technique using a homemade apparatus from a solution of

DOI: 10.1021/acsomega.7b01029
ACS Omega 2017, 2, 6975–6983

polymer blend composed of 20% of PA6 (w/v in respect to the solvent) in formic acid and 30% of PAH (w/w in respect to PA6). The solution was kept under magnetic stirring for 4 h at room temperature. The applied voltage was 25 kV and the distance between the needle (0.8 mm diameter) and the collector was 3 cm. The ejection rate was set at 0.01 mL h^{-1}. Random polymeric nanofibers were deposited on glass electrodes coated with indium tin oxide (ITO) and fluorine tin oxide attached to the cylindrical collector rotating at a speed of 250 rpm. The amount of nanofibers deposited onto the electrode was controlled by varying the spinning time.[23] The choice of these parameters for obtaining the electrospun fibers was based on prior works.[23]

4.2. Incorporation of MWCNTs onto PA6/PAH Nanofibers Surface. The electrospun nanofibers had their surface modified with the adsorption of MWCNTs from a 0.5 mg mL^{-1} dispersion in an ultrapure water, adding Triton X-100 (0.3% w/v) as a nonionic surfactant to improve dispersion, following the methodology described by Mercante et al.[23] The mixture was sonicated with an ultrasonic apparatus in an ice bath with an average power of 30 W for 120 min. After sonication, the PA6/PAH nanofibers were immersed in MWCNTs dispersion for 30 min. The fibers were then washed with distilled water and dried at room temperature.[23] A solution containing 0.1 mol L^{-1} *N*-ethyl-*N*-(3-dimethylaminopropyl) carbodiimide (EDC) and 0.1 mol L^{-1} *N*-hydroxysuccinimide (NHS) (1:1) was used for modifying the carboxylic acid groups of MWCNTs to allow for the binding with the antibody anti-CA19-9. Finally, the film was immersed into 1% bovine serum albumin (BSA) to block nonspecific binding sites.

4.3. Adsorption of Gold Nanoparticles onto PA6/PAH Nanofibers Surface. In another type of functionalization employed, PA6/PAH nanofibers were coated with a layer of gold nanoparticles (AuNPs)[23] (Figure 6). These citrate-functionalized AuNPs were synthesized using the Turkevich method,[55] in which 20 mL of 1 mM solution of $HAuCl_4$ was heated to 90 °C and 2 mL of 1% sodium citrate solution was added under vigorous stirring and constant heating. The solution changed color from yellowish ($HAuCl_4$) to red, indicating the Au nanoparticle formation. Heating was discontinued with continuous stirring of the solution till room temperature. The nanofibers were immersed in the solution of AuNPs for 12 h, and the nanoparticles were adsorbed onto the nanofibers surface by hydrogen bonding and electrostatic interactions.[23] The nanofibers were then washed with ultrapure water and dried at room temperature. The same procedure as mentioned above was performed with EDC/NHS to allow for the binding with the antibody anti-CA19-9, followed by the incorporation of BSA.

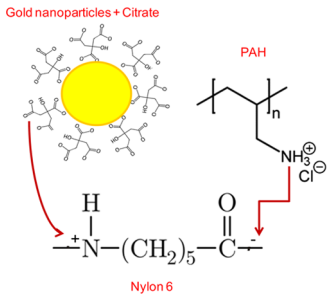

Figure 6. Schematic diagram for the binding between Nylon 6 (PA6), PAH, and gold nanoparticle.

4.4. Electrochemical Impedance Spectroscopy Measurements. Detection of CA19-9 biomarker was carried out using electrochemical impedance spectroscopy with the immunosensors manufactured as described in the previous subsections. The immunosensors were exposed to different concentrations of commercial CA19-9 biomarker for 10 min, followed by washing for the removal of poorly adsorbed molecules. In another set of experiments, the immunosensors were exposed to 4 blood serum samples from the pancreatic cancer patients of Barretos Cancer Hospital for 10 min, also followed by washing with PBS buffer. All of the experiments were performed using a PGSTAT 204 Autolab system containing a thermostated glass cell with a three-electrode configuration: ITO glass modified with the nanofiber mats employed as the working electrode, an Ag/AgCl electrode as a reference, and platinum foil as auxiliary electrode. The data were acquired in the frequency range between 1 and 10^6 Hz with a 10 mV amplitude.

AUTHOR INFORMATION

Corresponding Author

*E-mail: chu@ifsc.usp.br.

ORCID

Juliana C. Soares: 0000-0001-5455-1770
Andrey C. Soares: 0000-0003-4601-3555
Valquiria C. Rodrigues: 0000-0002-3738-3549
Matias E. Melendez: 0000-0002-0643-6185
Rui M. Reis: 0000-0002-9639-7940
Andre L. Carvalho: 0000-0001-7214-6402
Daniel S. Corrêa: 0000-0002-5592-0627

Notes

The authors declare no competing financial interest.

ACKNOWLEDGMENTS

This work was supported by FAPESP (Grant 2013/14262-7), CNPq, and CAPES (Brazil). D.S.C. also thanks FAPESP (Grant 2014/16789-5), Embrapa−Rede Agronano, and MCTI SisNano for financial support.

REFERENCES

(1) Yalow, R. S.; Berson, S. A. Assay of Plasma Insulin in Human Subjects by Immunological Methods. *Nature* **1959**, *184*, 1648−1649.
(2) Ekins, R. P. The Estimation of Thyroxine in Human Plasma by an Electrophoretic Technique. *Clin. Chim. Acta* **1960**, *5*, 453−459.
(3) Morgan, C. L.; Newman, D. J.; Price, C. P. Immunosensors: Technology and Opportunities in Laboratory Medicine. *Clin. Chem.* **1996**, *42*, 193−209.
(4) Lequin, R. M. Enzyme Immunoassay (EIA)/Enzyme-Linked Immunosorbent Assay (ELISA). *Clin. Chem.* **2005**, *51*, 2415−2418.
(5) Ricci, F.; Adornetto, G.; Palleschi, G. A Review of Experimental Aspects of Electrochemical Immunosensors. *Electrochim. Acta* **2012**, *84*, 74−83.
(6) Rabbany, S. Y.; Donner, B. L.; Ligler, F. S. Optical Immunosensors. *Crit. Rev. Biomed. Eng.* **1994**, *22*, 307−346.
(7) Aurich, K.; Glöckl, G.; Nagel, S.; Weitschies, W. Magneto-Optical Relaxation Measurements of Functionalized Nanoparticles as a Novel Biosensor. *Sensors* **2009**, *9*, 4022−4033.
(8) Soares, J. C.; Shimizu, F. M.; Soares, A. C.; Caseli, L.; Ferreira, J.; Oliveira, O. N. Supramolecular Control in Nanostructured Film Architectures for Detecting Breast Cancer. *ACS Appl. Mater. Interfaces* **2015**, *7*, 11833−11841.

DOI: 10.1021/acsomega.7b01029
ACS Omega 2017, 2, 6975−6983

(9) Soares, J. C.; Soares, A. C.; Pereira, P. A. R.; Rodrigues, V. d. C.; Shimizu, F. M.; Melendez, M. E.; Scapulatempo Neto, C.; Carvalho, A. L.; Leite, F. L.; Machado, S. A. S.; Oliveira, O. N. Adsorption according to the Langmuir−Freundlich Model Is the Detection Mechanism of the Antigen p53 for Early Diagnosis of Cancer. *Phys. Chem. Chem. Phys.* **2016**, *18*, 8412−8418.
(10) Soares, A. C.; Soares, J. C.; Shimizu, F. M.; Melendez, M. E.; Carvalho, A. L.; Oliveira, O. N. Controlled Film Architectures to Detect a Biomarker for Pancreatic Cancer Using Impedance Spectroscopy. *ACS Appl. Mater. Interfaces* **2015**, *7*, 25930−25937.
(11) Bhakta, S. A.; Evans, E.; Benavidez, T. E.; Garcia, C. D. Protein Adsorption onto Nanomaterials for the Development of Biosensors and Analytical Devices: A Review. *Anal. Chim. Acta* **2015**, *872*, 7−25.
(12) Ahmad, A.; Moore, E. Electrochemical Immunosensor Modified with Self-Assembled Monolayer of 11-Mercaptoundecanoic Acid on Gold Electrodes for Detection of Benzo[a]pyrene in Water. *Analyst* **2012**, *137*, 5839.
(13) Gurard-Levin, Z. A.; Mrksich, M. Combining Self-Assembled Monolayers and Mass Spectrometry for Applications in Biochips. *Annu. Rev. Anal. Chem.* **2008**, *1*, 767−800.
(14) Decher, G.; Hong, J.-D. Buildup of Ultrathin Multilayer Films by a Self-Assembly Process, 1 Consecutive Adsorption of Anionic and Cationic Bipolar Amphiphiles on Charged Surfaces. *Makromol. Chem., Macromol. Symp.* **1991**, *46*, 321−327.
(15) Berzina, T.; Piras, L.; Troitsky, V. Study of Horseradish Peroxidase Activity in Alternate-Layer Langmuir−Blodgett Films. *Thin Solid Films* **1998**, *327−329*, 621−626.
(16) Godoy, S.; Violot, S.; Boullanger, P.; Bouchu, M.-N.; Leca-Bouvier, B. D.; Blum, L. J.; Girard-Egrot, A. P. Kinetics Study of Bungarus Fasciatus Venom Acetylcholinesterase Immobilised on a Langmuir-Blodgett Proteo-Glycolipidic Bilayer. *ChemBioChem* **2005**, *6*, 395−404.
(17) Godoy, S.; Chauvet, J.-P.; Boullanger, P.; Blum, L. J.; Girard-Egrot, A. P. New Functional Proteo-Glycolipidic Molecular Assembly for Biocatalysis Analysis of an Immobilized Enzyme in a Biomimetic Nanostructure. *Langmuir* **2003**, *19*, 5448−5456.
(18) Gan, N.; Zhou, J.; Xiong, P.; Li, T.; Jiang, S.; Cao, Y.; Jiang, Q. An Ultrasensitive Electrochemiluminescence Immunoassay for Carbohydrate Antigen 19-9 in Serum Based on Antibody Labeled Fe3O4 Nanoparticles as Capture Probes and Graphene/CdTe Quantum Dot Bionanoconjugates as Signal Amplifiers. *Int. J. Mol. Sci.* **2013**, *14*, 10397−10411.
(19) Mehta, J.; Vinayak, P.; Tuteja, S. K.; Chhabra, V. A.; Bhardwaj, N.; Paul, A. K.; Kim, K.-H.; Deep, A. Graphene Modified Screen Printed Immunosensor for Highly Sensitive Detection of Parathion. *Biosens. Bioelectron.* **2016**, *83*, 339−346.
(20) Singh, M.; Holzinger, M.; Tabrizian, M.; Winters, S.; Berner, N. C.; Cosnier, S.; Duesberg, G. S. Noncovalently Functionalized Monolayer Graphene for Sensitivity Enhancement of Surface Plasmon Resonance Immunosensors. *J. Am. Chem. Soc.* **2015**, *137*, 2800−2803.
(21) Xie, Y.; Chen, A.; Du, D.; Lin, Y. Graphene-Based Immunosensor for Electrochemical Quantification of Phosphorylated p53 (S15). *Anal. Chim. Acta* **2011**, *699*, 44−48.
(22) Huang, Z.; Wang, X.; Yang, D. Adsorption of Cr(VI) in Wastewater Using Magnetic Multi-Wall Carbon Nanotubes. *Water Sci. Eng.* **2015**, *8*, 226−232.
(23) Mercante, L. A.; Pavinatto, A.; Iwaki, L. E. O.; Scagion, V. P.; Zucolotto, V.; Oliveira, O. N.; Mattoso, L. H. C.; Correa, D. S. Electrospun Polyamide 6/Poly(allylamine Hydrochloride) Nanofibers Functionalized with Carbon Nanotubes for Electrochemical Detection of Dopamine. *ACS Appl. Mater. Interfaces* **2015**, *7*, 4784−4790.
(24) Sánchez, S.; Fàbregas, E.; Pumera, M. Detection of Biomarkers with Carbon Nanotube-Based Immunosensors. In *Carbon Nanotubes*; Balasubramanian, K., Burghard, M., Eds.; Humana Press: Totowa, NJ, 2010; pp 227−237.
(25) Veetil, J. V.; Ye, K. Development of Immunosensors Using Carbon Nanotubes. *Biotechnol. Prog.* **2007**, *23*, 517−531.
(26) Anik, Ü.; Timur, S. Towards the Electrochemical Diagnosis of Cancer: Nanomaterial-Based Immunosensors and Cytosensors. *RSC Adv.* **2016**, *6*, 111831−111841.
(27) El-Dib, F. I.; Hussein, M. H. M.; Hefni, H. H. H.; Eshaq, G.; ElMetwally, A. E. Synthesis and Characterization of Crosslinked Chitosan Immobilized on Bentonite and Its Grafted Products with Polyaniline. *J. Appl. Polym. Sci.* **2014**, *131*, 1−7.
(28) Luo, Y.; Wang, S.; Shen, M.; Qi, R.; Fang, Y.; Guo, R.; Cai, H.; Cao, X.; Tomás, H.; Zhu, M.; Shi, X. Carbon Nanotube-Incorporated Multilayered Cellulose Acetate Nanofibers for Tissue Engineering Applications. *Carbohydr. Polym.* **2013**, *91*, 419−427.
(29) Hu, D.; Huang, Y.; Liu, H.; Wang, H.; Wang, S.; Shen, M.; Zhu, M.; Shi, X. The Assembly of Dendrimer-Stabilized Gold Nanoparticles onto Electrospun Polymer Nanofibers for Catalytic Applications. *J. Mater. Chem. A* **2014**, *2*, 2323.
(30) Sidik, N. A. C.; Yazid, M. N. A. W. M.; Samion, S. A Review on the Use of Carbon Nanotubes Nanofluid for Energy Harvesting System. *Int. J. Heat Mass Transfer* **2017**, *111*, 782−794.
(31) Cao, X.; Ye, Y.; Liu, S. Gold Nanoparticle-Based Signal Amplification for Biosensing. *Anal. Biochem.* **2011**, *417*, 1−16.
(32) Mercante, L. A.; Scagion, V. P.; Migliorini, F. L.; Mattoso, L. H. C.; Correa, D. S. Electrospinning-Based (Bio)sensors for Food and Agricultural Applications: A Review. *TrAC, Trends Anal. Chem.* **2017**, *91*, 91−103.
(33) Jiang, Z.; Zhao, C.; Lin, L.; Weng, S.; Liu, Q.; Lin, X. A Label-Free Electrochemical Immunosensor Based on poly(thionine)−SDS Nanocomposites for CA19-9 Detection. *Anal. Methods* **2015**, *7*, 4508−4513.
(34) Ballehaninna, U. K.; Chamberlain, R. S. Serum CA 19-9 as a Biomarker for Pancreatic Cancer—A Comprehensive Review. *Indian J. Surg. Oncol.* **2011**, *2*, 88−100.
(35) Ballehaninna, U. K.; Chamberlain, R. S. The Clinical Utility of Serum CA 19-9 in the Diagnosis, Prognosis and Management of Pancreatic Adenocarcinoma: An Evidence Based Appraisal. *J. Gastrointest. Oncol.* **2012**, *3*, 105−119.
(36) International Agency for Research on Cancer. The Pancreatic Cancer Working Group. http://epic.iarc.fr/research/cancerworkinggroups/pancreaticcancer.php (accessed May 30, 2017).
(37) Zhang, Q.; Chen, X.; Tang, Y.; Ge, L.; Guo, B.; Yao, C. Amperometric Carbohydrate Antigen 19-9 Immunosensor Based on Three Dimensional Ordered Macroporous Magnetic Au Film Coupling Direct Electrochemistry of Horseradish Peroxidase. *Anal. Chim. Acta* **2014**, *815*, 42−50.
(38) Huang, Z.; Jiang, Z.; Zhao, C.; Han, W.; Lin, L.; Liu, A.; Weng, S.; Lin, X. Simple and Effective Label-Free Electrochemical Immunoassay for Carbohydrate Antigen 19-9 Based on Polythionine-Au Composites as Enhanced Sensing Signals for Detecting Different Clinical Samples. *Int. J. Nanomed.* **2017**, *12*, 3049−3058.
(39) Zhang, A.; Xiang, H.; Zhang, X.; Guo, W.; Yuan, E.; Huang, C.; Jia, N. A Novel Sandwich Electrochemiluminescence Immunosensor for Ultrasensitive Detection of Carbohydrate Antigen 19-9 Based on Immobilizing Luminol on Ag@BSA Core/Shell Microspheres. *Biosens. Bioelectron.* **2016**, *75*, 206−212.
(40) Zhang, W.; Du, Y.; Wang, M. L. On-Chip Highly Sensitive Saliva Glucose Sensing Using Multilayer Films Composed of Single-Walled Carbon Nanotubes, Gold Nanoparticles, and Glucose Oxidase. *Sens. Bio-Sens. Res.* **2015**, *4*, 96−102.
(41) Rahmani, M.; Lukiyanchuk, B.; Tahmasebi, T.; Lin, Y.; Liew, T. Y. F.; Hong, M. H. Polarization-Controlled Spatial Localization of near-Field Energy in Planar Symmetric Coupled Oligomers. *Appl. Phys. A* **2012**, *107*, 23−30.
(42) Paulovich, F. V.; Moraes, M. L.; Maki, R. M.; Ferreira, M.; Oliveira, O. N., Jr.; de Oliveira, M. C. F. Information Visualization Techniques for Sensing and Biosensing. *Analyst* **2011**, *136*, 1344.
(43) Lvovich, V. F. *Impedance Spectroscopy: Applications to Electrochemical and Dielectric Phenomena*; John Wiley & Sons: Hoboken, 2012; pp 13−20.

DOI: 10.1021/acsomega.7b01029
ACS Omega 2017, 2, 6975−6983

(44) Currie, L. A. Nomenclature in Evaluation of Analytical Methods Including Detection and Quantification capabilities[1]: (IUPAC Recommendations 1995). *Anal. Chim. Acta* **1999**, *391*, 105−126.
(45) Passerini, R.; Riggio, D.; Salvatici, M.; Zorzino, L.; Radice, D.; Sandri, M. T. Interchangeability of Measurements of CA 19-9 in Serum with Four Frequently Used Assays: An Update. *Clin. Chem. Lab. Med.* **2007**, *45*, 100−104.
(46) Yang, F.; Yang, Z.; Zhuo, Y.; Chai, Y.; Yuan, R. Ultrasensitive Electrochemical Immunosensor for Carbohydrate Antigen 19-9 Using Au/Porous Graphene Nanocomposites as Platform and Au@Pd Core/Shell Bimetallic Functionalized Graphene Nanocomposites as Signal Enhancers. *Biosens. Bioelectron.* **2015**, *66*, 356−362.
(47) Zhang, Q.; Chen, X.; Tang, Y.; Ge, L.; Guo, B.; Yao, C. Amperometric Carbohydrate Antigen 19-9 Immunosensor Based on Three Dimensional Ordered Macroporous Magnetic Au Film Coupling Direct Electrochemistry of Horseradish Peroxidase. *Anal. Chim. Acta* **2014**, *815*, 42−50.
(48) Rodrigues, V. d. C.; Comin, C. H.; Soares, J. C.; Soares, A. C.; Melendez, M. E.; Fregnani, J. H. T. G.; Carvalho, A. L.; Costa, L. d. F.; Oliveira, O. N. Analysis of Scanning Electron Microscopy Images To Investigate Adsorption Processes Responsible for Detection of Cancer Biomarkers. *ACS Appl. Mater. Interfaces* **2017**, *9*, 5885−5890.
(49) Colthup, N. B.; Lawrence, H. D.; Stephen, E. W. *Introduction to Infrared and Raman Spectroscopy*; Academic Press: San Diego, 1990; pp 184−210.
(50) Riul, A.; dos Santos, D. S.; Wohnrath, K.; Di Tommazo, R.; Carvalho, A. C. P. L. F.; Fonseca, F. J.; Oliveira, O. N.; Taylor, D. M.; Mattoso, L. H. C. Artificial Taste Sensor: Efficient Combination of Sensors Made from Langmuir−Blodgett Films of Conducting Polymers and a Ruthenium Complex and Self-Assembled Films of an Azobenzene-Containing Polymer. *Langmuir* **2002**, *18*, 239−245.
(51) Jeppu, G. P.; Clement, T. P. A Modified Langmuir-Freundlich Isotherm Model for Simulating pH-Dependent Adsorption Effects. *J. Contam. Hydrol.* **2012**, *129−130*, 46−53.
(52) Adamson, A. W.; Gast, A. P. *Physical Chemistry of Surfaces*; Wiley: New York, 1997; pp 603−614.
(53) Turiel, E.; Perez-Conde, C.; Martin-Esteban, A. Assessment of the Cross-Reactivity and Binding Sites Characterisation of a Propazine-Imprinted Polymer Using the Langmuir-Freundlich Isotherm. *Analyst* **2003**, *128*, 137−141.
(54) Zhang, P.; Wang, L. Extended Langmuir Equation for Correlating Multilayer Adsorption Equilibrium Data. *Sep. Purif. Technol.* **2010**, *70*, 367−371.
(55) Kimling, J.; Maier, M.; Okenve, B.; Kotaidis, V.; Ballot, H.; Plech, A. Turkevich Method for Gold Nanoparticle Synthesis Revisited. *J. Phys. Chem. B* **2006**, *110*, 15700−15707.

DOI: 10.1021/acsomega.7b01029
ACS Omega 2017, 2, 6975−6983